ELSEVIER

Journal of Materials Processing Technology 170 (2005) 89–96

Journal of Materials Processing Technology

www.elsevier.com/locate/jmatprotec

Microstructures and mechanical properties of Fe–15% Cr–15% Ni austenitic stainless steels containing different levels of niobium additions submitted to various processing stages

Angelo Fernando Padilha [a,*], Izabel Fernanda Machado [b], Ronald Lesley Plaut [a]

[a] *Universidade de São Paulo, Departamento de Engenharia Metalúrgica e de Materiais, Av. Prof. Mello Moraes, 2463, São Paulo 05508-900, Brazil*

[b] *Universidade de São Paulo, Departamento de Engenharia Mecatrônica e Sistemas Mecânicos, Av. Prof. Mello Moraes, 2231, São Paulo 05508-900, Brazil*

Received 23 December 2004; accepted 9 May 2005

Abstract

In this work additions of 0.5, 1.0 and 2.0 wt.% of niobium were made to a Fe–15% Cr–15% Ni austenitic stainless steel. The microstructures and the mechanical properties of the as cast, hot forged, solution annealed and aged samples as well as the tape alloys (produced using the melt spinning process) were evaluated and compared. The microstructures of the steels were characterized and analyzed using several complementary techniques. Mechanical properties were measured using tensile tests and Vickers hardness. Results showed that niobium additions caused an enlargement of the solidification interval and led to Laves phase formation in the as cast samples. The Laves phase is hard and fragile and its formation between austenite dendrites caused loss in toughness and ductility. After hot forging, the microstructure of the samples was essentially constituted by recrystallized austenitic grains and a relative uniform dispersion of Laves phase particles in the alloys containing niobium. The samples were solution annealed at 1200 or at 1250 °C after hot forging. Annealing did not allow a complete dissolution of particles observed in the hot forged samples whereas the melt spinning process produced alloys free of Laves phase particles. Aging of niobium containing alloys in the temperature range between 600 and 800 °C caused significant precipitation hardening.

Keywords: Austenitic stainless steel; Niobium additions; Laves phase; Microstructure; Mechanical properties

1. Introduction

Fe–15% Cr–15% Ni austenitic stainless steels have a fully austenitic microstructure which is free of δ-ferrite and intermetallic phases such as sigma (σ) and chi (χ) phases, due to their low Cr/Ni ratio and the absence of molybdenum [1–5]. Fully austenitic stainless steels, particularly the 15% Cr–15% Ni type [6,7], are employed in high temperature applications in which creep and oxidation resistance plus microstructural stability are mandatory [8]. Formation of strain-induced martensite is not observed in the Fe–15% Cr–15% Ni austenitic stainless steels [1–7]. In ferritic stainless steels, recent work [9,10] has shown the effect of niobium addition, mainly on Laves phase formation [9] and its dissolution [10]. In austenitic stainless steels, niobium reacts with carbon resulting in NbC and thereby hindering the precipitation of $M_{23}C_6$, reducing the susceptibility to intergranular corrosion. In niobium-stabilized austenitic steel primary NbC formation was also observed during solidification [4]. Laves phase is also favored in austenitic stainless steels by niobium additions [11–15]. For niobium levels up to 0.07% the solubility limit in the austenitic stainless steel is sufficient [11] to cause Laves phase (Fe_2Nb) formation. Precipitation hardening can occur if the precipitated Laves phase shows a coherent or semi-coherent interface with the matrix [12,13]. However, the Laves phase frequently shows deleterious effects on mechanical properties because it is hard and fragile, hence causing loss of toughness. In this work, nominal additions

* Corresponding author. Tel.: +55 11 30915239; fax: +55 11 30915243.
E-mail addresses: padilha@usp.br (A.F. Padilha), machadoi@usp.br (I.F. Machado).

0924-0136/$ – see front matter © 2005 Elsevier B.V. All rights reserved.
doi:10.1016/j.jmatprotec.2005.05.002

of 0.5, 1.0 and 2.0 wt.% of niobium were made to the fully austenitic Fe–15% Cr–15% Ni austenitic stainless steel. The objective of the present study is to compare the effect of niobium additions to the Fe–15% Cr–15% Ni austenitic stainless steel in terms of microstructure and mechanical properties. The alloys were characterized and analyzed in the as cast, hot forged, annealed, aged and after rapid solidification conditions (melt spinning). The carbon in the studied alloys was kept below 0.03% to minimize the NbC precipitation. Residual elements like P, S, Cu, Sn and As were also kept at very low levels. Alloy microstructures were analyzed using several complementary techniques such as differential thermo analysis, precipitate extraction, X-ray diffraction, optical, scanning (with energy dispersive X-ray spectroscopy) and transmission electron microscopy. The presence of magnetic phases was evaluated using a ferritoscope. Mechanical properties were also determined for the Fe–15% Cr–15% Ni–Nb samples using tensile test and Vickers hardness measurements.

2. Materials and methods

The alloys with different niobium contents were prepared by vacuum induction melting (VIM) from high purity raw materials. The chemical compositions of the alloys are given in Table 1.

The as cast alloys were characterized and hot forged in the temperature range of 1000 and 1200 °C. As a result, bars of about 20 mm diameter were produced. Subsequently, the bars were solution annealed at 1200 °C for 1 h or at 1250 °C for 3 h. The samples solution annealed at 1250 °C for 3 h were aged at 600, 700 and 800 °C for up to 300 h.

Tapes of Fe–15% Cr–15% Ni–Nb alloys were also produced using the melt spinning process. These tapes were generated using 6 g samples of each alloy that were induction melted in a ceramic crucible in an atmosphere of 0.3 helium bar. The melted alloys were propelled with a speed of 20 m/s, under a pressure of 0.5 argon bar, against a rotating copper wheel. The estimated cooling rate was about 10^5–10^6 K/s. Tape dimensions were 4 mm width and 40–80 μm thickness.

Table 1
Chemical compositions of the Fe–15% Cr–15% Ni–Nb (in wt.%) alloys

Element	N00	N05	N10	N20a	N20b
C	0.02	0.02	0.02	0.02	0.03
Si	0.59	0.48	0.53	0.57	0.41
Mn	0.53	0.43	0.52	0.47	0.51
P	0.006	0.006	0.006	0.006	0.006
S	0.013	0.012	0.012	0.012	0.008
Cu	0.02	0.04	0.01	0.01	0.02
Cr	14.4	14.7	15.1	14.6	13.4
Al	<0.005	<0.005	<0.005	0.005	0.013
Sn	0.002	0.002	0.001	0.001	0.001
As	0.002	0.001	0.002	0.002	0.004
Ni	15.0	15.1	14.8	14.8	15.2
N	0.0084	0.0081	0.0075	0.0081	0.028
Mo	0.01	0.01	<0.01	<0.01	<0.01
Nb	<0.002	0.44	0.89	1.74	1.88

Microstructures of the alloys were observed using optical microscopy (OM), scanning electron microscopy (SEM) with energy dispersive X-ray spectroscopy (EDS) and transmission electron microscopy (TEM). Metallographic sample preparation for OM and SEM observations consisted of grinding down to 2400-grit paper, followed by 1 μm diamond polishing with further electrolytic polishing. The composition of the polishing electrolyte was 950 ml acetic acid and 50 ml perchloric acid. The electrolyte was kept at 13 °C and the samples were polished at 80 V for 80 s. After electrolytic polishing, the samples were etched with V2A-Beize [16] at 70 °C for 20–60 s. Compositions of the different phases were determined by energy dispersive analysis. For TEM observation, the samples were mechanically thinned down to 150 μm and then punched into 3 mm discs. The thin-foil samples were produced by electropolishing the discs in 100 ml perchloric acid (60%), 200 ml glycerin and 700 ml methanol. The electrolyte was kept at −30 °C and 0.3–0.4 A were applied for few seconds. Following, thin foil samples were cleaned with water, alcohol and dried in air. The crystal structures of the different phases were determined: (a) by electron diffraction pattern utilizing TEM; (b) by X-ray diffractometry on polished surfaces and (c) by analysis of Debye-Scherrer camera data of the extracted residue after dissolution of the matrix. In the two last cases, Mo Kα radiation was used. The presence of magnetic phases, if any, was determined by using the magnetic induction method (a ferritoscope with 0.1% detection limit).

Tensile tests were carried out to determine mechanical properties as yield point, tensile strength and total elongation. Tensile tests were performed on round bar samples with 5 mm diameter and 25 mm gauge length. A special kind of mechanical test was also carried out to evaluate the toughness (crack propagation) of the studied steels, which consisted of compressing the metallographically prepared samples. Fig. 1 shows schematically the sample and the forces applied to the above mentioned special test specimen. Using this test, crack propagation path could be easily observed on the X-surface. Vickers hardness using a load of 100 N was used to compare the studied alloys in different conditions. In the case of melt spinned alloys (tapes) Vickers hardness load was 0.15 N.

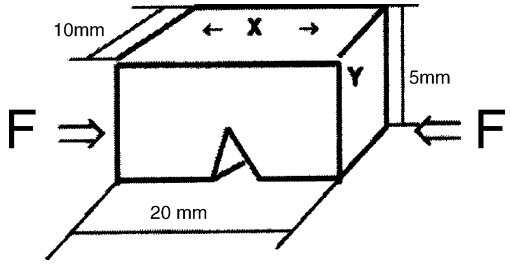

Fig. 1. Schematic drawing of the sample for mechanical testing. X is the metallographically prepared surface. Y is the surface where compression force (F) was applied.

Differential thermal analysis (DTA) was utilized to determine the effect of niobium additions on the *solidus* and *liquidus* lines. Samples (1 g) were analyzed using alumina crucibles. Results were obtained in the temperature range of 1100 and 1500 °C. Heating and cooling rates were 10 °C/min.

3. Results

Using DTA it was verified that niobium additions caused a depression of the *liquidus* and *solidus* lines with a simultaneous enlargement of the solidification interval, as shown in Fig. 2.

Niobium additions also led to modifications in the microstructure of the Fe–15% Cr–15% Ni system. Different mechanical properties are expected in the alloys studied as a consequence of changes in composition and microstructure. For the sake of simplicity results will be presented in two sections: microstructure and mechanical properties.

3.1. Microstructure

In the as cast steels samples, the results indicated the absence of magnetism. On the other hand, an intermetallic phase was detected in the four steels containing niobium. The amount of the intermetallic phase could be related to the niobium content. In the high niobium alloys (N10, N20a and N20b) the intermetallic phase formed a continuous network and the volumetric fraction was proportional to niobium wt.%. Figs. 3 and 4 show the microstructure of the as cats steel sample containing about 2 wt.% of niobium.

Energy dispersive analysis of the intermetallic phase revealed high iron and niobium contents and low nickel, chromium and silicon contents. On the other hand, matrix analysis indicated the absence of niobium. In the as cast Fe–15% Cr–15% Ni–Nb alloys almost all niobium was concentrated in the particles. Table 2 shows the results of chemical composition of these particles in the studied steels. The intermetallic phase formed during solidification was identified as Laves phase by analyzing X-ray diffraction data of the extracted residues. Lattice parameters of Laves phase, $(Fe,Ni,Cr)_2(Nb,Si)$, of this work were $a = 0.476$ nm and $c = 0.786$ nm. A more detailed examination of the microstructure also revealed the presence of small quantities of NbC and mixed oxide particles. Fig. 5 shows schematically a proposed section of the Fe–15% Cr–15% Ni–0.03% C–Nb phase diagram.

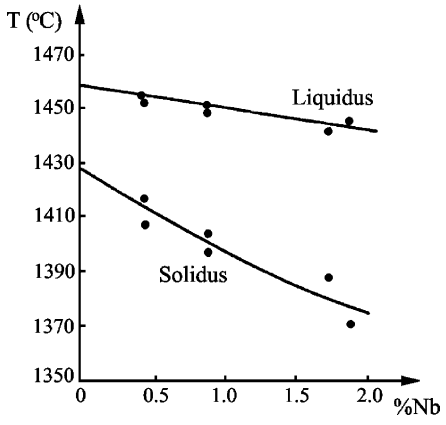

Fig. 2. Effect of niobium additions on the *liquidus* and *solidus* lines of Fe–15% Cr–15% Ni system.

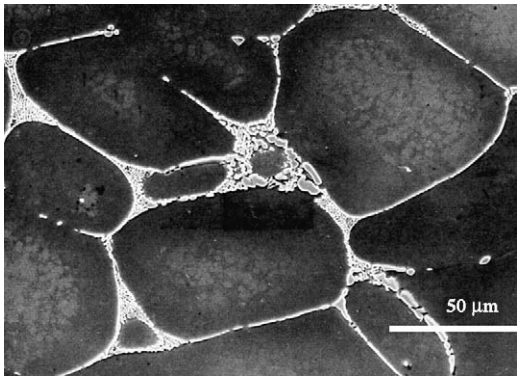

Fig. 3. As cast sample containing about 2 wt.% of niobium (N20a). Scanning electron microscopy. Secondary electrons image. Etching: V2A-Beize.

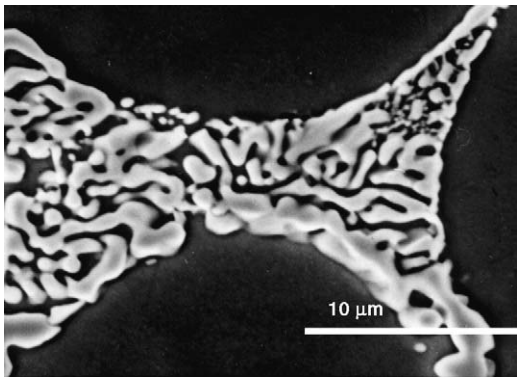

Fig. 4. As cast sample containing about 2 wt.% of niobium (N20a). Scanning electron microscopy. Secondary electrons image. Etching: V2A-Beize. Details of the micrograph of Fig. 3.

The as cast alloys were subsequently hot forged (between 1000 and 1200 °C) with an area reduction of about 95%, giving an average grain diameter of about 20 μm.

Fig. 6 shows a micrograph of the alloy containing about 2 wt.% niobium in the hot forged condition. The microstructure after forging showed essentially recrystallized grains. The alloys containing niobium showed a relatively

Table 2
Chemical composition of the Laves phase in the studied steels determined by EDS analysis

Element	(at.%)	(wt.%)
Fe	46.5 ± 0.9	41.6 ± 1.0
Ni	12.6 ± 0.5	11.9 ± 0.5
Cr	11.3 ± 0.3	9.4 ± 0.3
Nb	22.9 ± 0.7	34.9 ± 0.9
Si	6.8 ± 0.2	3.1 ± 0.1

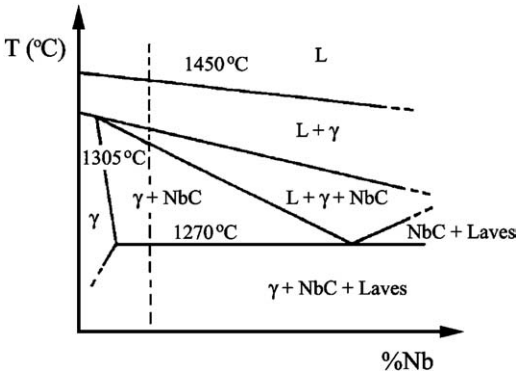

Fig. 5. Schematic proposed representation of a section of the Fe–15% Cr–15% Ni–0.03% C–Nb phase diagram.

non-uniform dispersion of Laves phase particles smaller than 10 μm. Hot forging caused fragmentation, redistribution and partial dissolution of some particles, hence increasing the niobium content in the matrix. For example, in the alloy N20b (1.89% Nb), about 40% of niobium in the alloy was in solid solution after forging. After hot forging, the alloys were annealed at 1200 °C for 1 h or at 1250 °C for 3 h leading to a significant dissolution of particles. However, a complete dissolution of particles even at these high temperatures was not observed.

Solution annealed samples were aged at 600, 700 and 800 °C for up to 300 h. Chromium carbide $(Cr,Fe)_{23}C_6$ precipitation occurred at grain boundaries in the niobium free alloy (N00). On the other hand, extensive Laves phase formation was observed in niobium containing alloys. Laves phase precipitated first at grain boundaries followed by precipitation at incoherent twin boundaries, coherent twin boundaries and grain interior, in that order. Laves phase particles having plate morphology can be observed in Figs. 7 and 8. Using TEM it was possible to determine the relationship between the austenitic matrix and the Laves phase as being: $(0\,0\,0\,1)Fe_2Nb//(1\,1\,1)\gamma$ and $[1\,0\,\bar{1}\,0]\,Fe_2Nb//[\bar{1}\,1\,0]\gamma$. Laves phase nucleation is sluggish but when it starts the precipitate growth is faster. In these micrographs it is interesting to observe that the coherent twin boundaries have been extensively covered by Laves phase, despite its late nucleation.

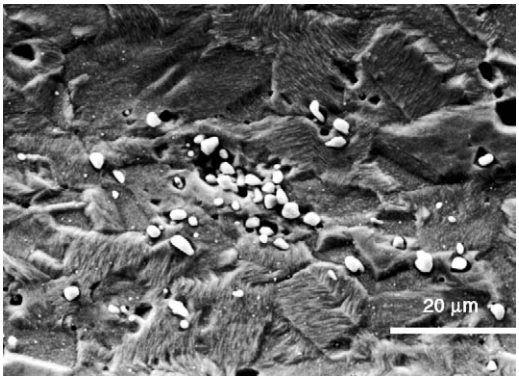

Fig. 6. Hot forged alloy containing about 2 wt.% niobium (N20a). Scanning electron microscopy. Secondary electrons image. Etching: V2A-Beize.

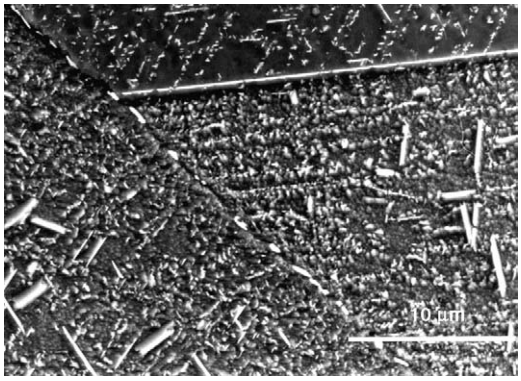

Fig. 7. Aged sample containing about 2 wt.% niobium (N20b). Aged at 700 °C for 100 h. Scanning electron microscopy. Secondary electrons image. Etching: V2A-Beize.

Melt spinning process was utilized to keep niobium dissolved in solid solution. Only fine grained austenite (average grain diameter of about 3 μm) was identified in all alloy tapes of the studied compositions, confirmed by scanning electron microscopy (see Fig. 9) and transmission electron

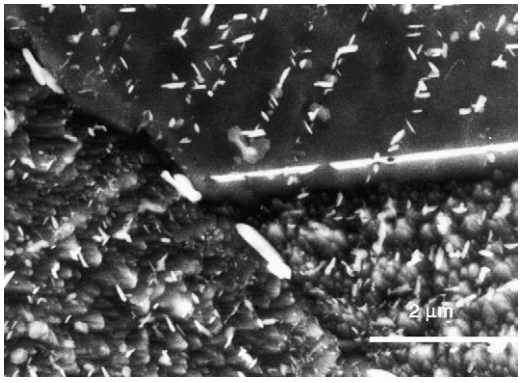

Fig. 8. Aged sample containing about 2 wt% niobium (N20b). Aged at 700 °C for 100 h. Scanning electron microscopy. Secondary electrons image. Etching: V2A-Beize.

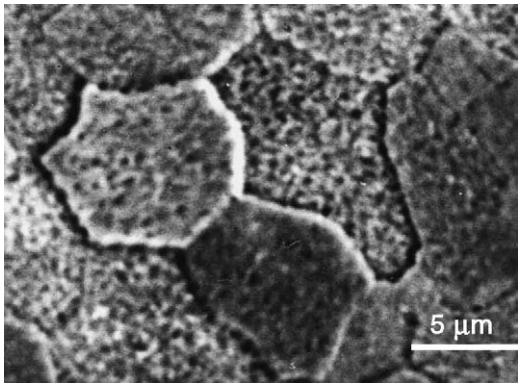

Fig. 9. Melt spinned tape alloy containing about 2 wt% niobium (N20b). Scanning electron microscopy. Secondary electrons image. Etching: V2A-Beize.

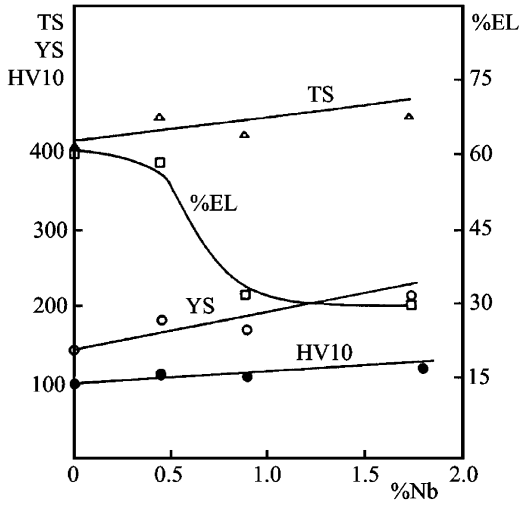

Fig. 10. Vickers hardness (HV 10), yield strength (YS, N/mm^2), tensile strength (TS, N/mm^2) and total elongation (EL, %) variation with niobium contents in the as cast steels.

microscopy. X-ray diffraction data further confirmed that niobium expanded the austenite lattice: the alloy without niobium had a lattice parameter of about 0.3549 nm whereas the alloys containing niobium had a parameter of about 0.3556 nm.

3.2. Mechanical properties

Fig. 10 presents the mechanical properties for the studied as cast steels with varying niobium contents. Using the special mechanical test specimen (see Fig. 1), crack propagation path could be observed easily. Figs. 11 and 12 show the micrographs of the high niobium as cast material where cracks can be seen within the Laves phase and that these propagate along eutectic colonies.

Fig. 13 shows the mechanical properties of the hot forged and solution annealed steels as a function of varying niobium contents. Comparing with the previous condition (see Fig. 10), a clear enhancement of the mechanical properties can be observed, mainly in the total elongation.

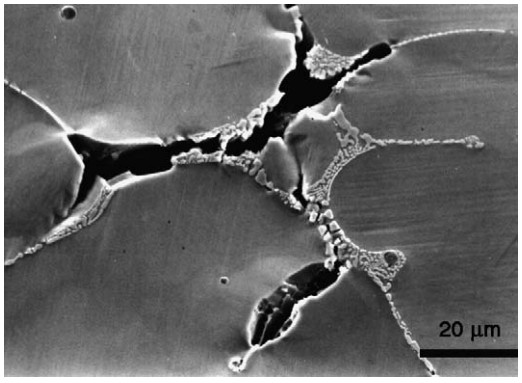

Fig. 11. As cast sample containing about 2 wt.% of niobium (N20b). Scanning electron microscopy after mechanical test. Secondary electrons image. Etching: V2A-Beize.

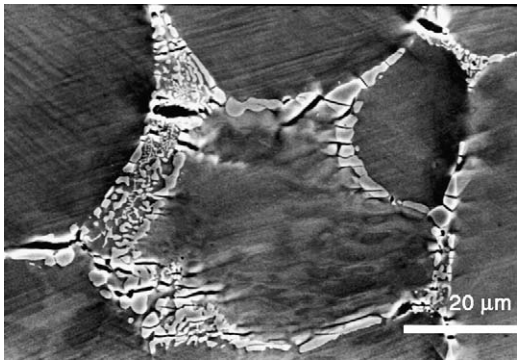

Fig. 12. As cast sample containing about 2 wt.% of niobium (N20b). Scanning electron microscopy after mechanical test. Secondary electrons image. Etching: V2A-Beize.

Fig. 14 shows the variation of the mechanical properties of the hot forged, solution-annealed (at 1250 °C for 3 h) and aged (at 700 °C for 100 h) samples as a function of niobium content. Comparing, once again, now with Fig. 13, one can observe improvements in yield strength, tensile strength and hardness, but significant deterioration in ductility (total elongation), due to solid state Laves phase precipitation.

In order to investigate the precipitation hardening behavior (using hardness measurements, HV 10), samples have been aged at 600, 700 and 800 °C up to 300 h. Figs. 15–17 show a hardness increase with aging time mainly for the higher niobium containing alloys. At the highest investigated temperature of 800 °C, an overaging effect was observed.

Mechanical properties of the tapes of the steels obtained by melt spinning process are known to be difficult to measure due to the tape dimensions, hence only Vickers microhardness have been measured in these tapes using a 0.15 N load. Table 3 compares the results of Vickers microhardness of three alloys in the conditions of melt spinned tapes and the corresponding hot forged and solution annealed ones. Despite the difference

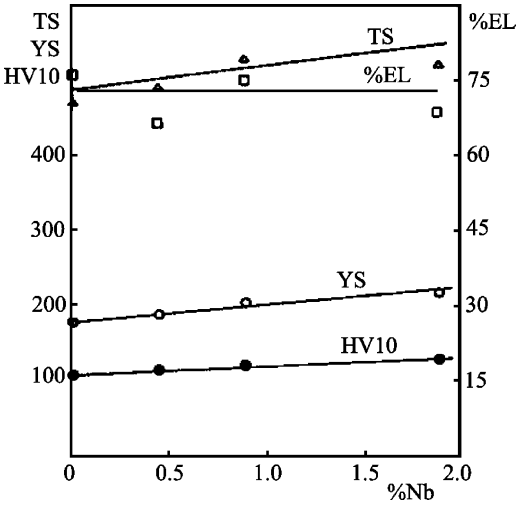

Fig. 13. Vickers hardness (HV 10), yield strength (YS, N/mm^2), tensile strength (TS, N/mm^2) and total elongation (EL, %) as a function of niobium content in the forged and solution-annealed (1 h at 1200 °C) steels.

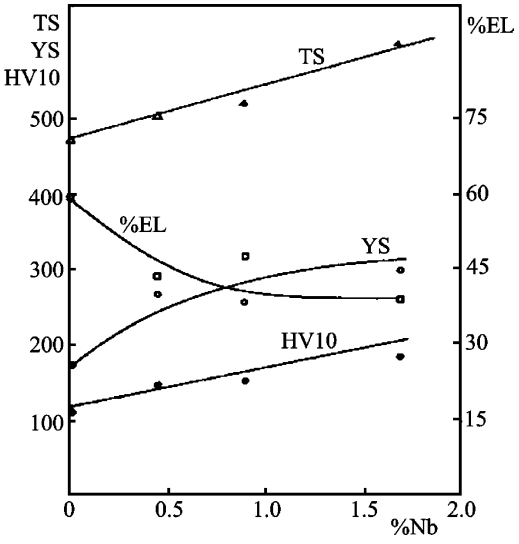

Fig. 14. Vickers hardness (HV 10), yield strength (YS, N/mm^2), tensile strength (TS, N/mm^2) and total elongation (EL, %) as a function of niobium contents in the steels solution-annealed at 1250 °C for 3 h and aged at 700 °C for 100 h.

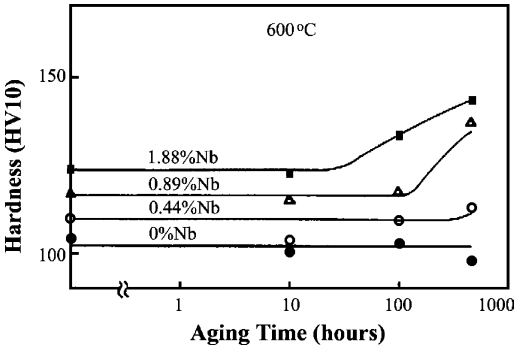

Fig. 15. Hardness vs. aging time. Alloys N00, N05, N10, N20b aged at 600 °C.

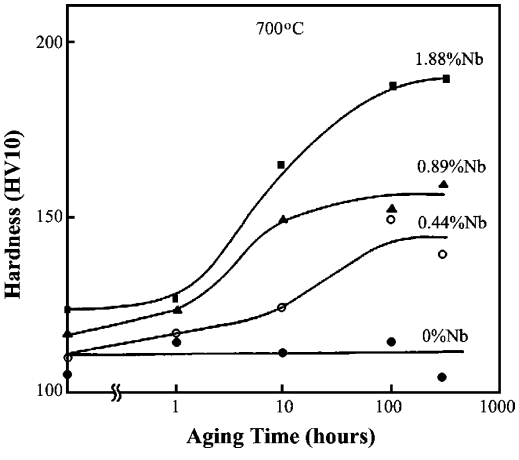

Fig. 16. Hardness vs. aging time. Alloys N00, N05, N10, N20b aged at 700 °C.

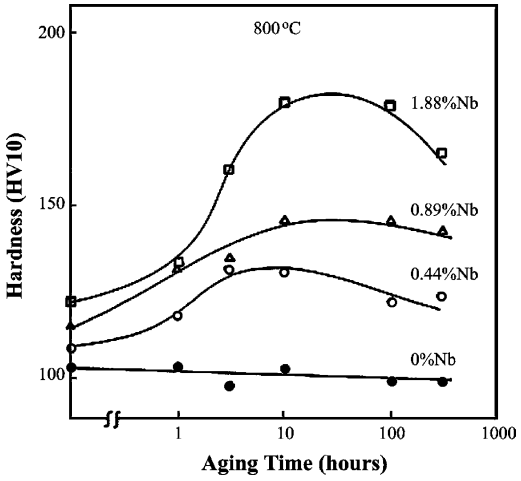

Fig. 17. Hardness vs. aging time. Alloys N00, N05, N10, N20b aged at 800 °C.

Table 3
Vickers hardness of tape alloys (HV 0.015) and of hot forged (HV 10) and solution-annealed (at 1250 °C for 3 h) samples

Alloy	Vickers microhardness (HV 0.015)	Vickers microhardness (HV 10)
N00	182	105
N10	196	117
N20b	247	124

in loads in the microhardness testing, it may be pointed out that the hardness increase was higher than 65% for each alloy. The largest hardness increase (about 100%), was noticed for the alloy (N20b), the largest niobium containing alloy.

4. Discussion

Based on DTA results (see Fig. 2), it may be observed that niobium additions caused an enlargement of the solidification interval, hence the niobium containing alloys are prone to interdendritic Laves phase formation. Similar phenomenon has been observed, by other authors [17], for molybdenum additions. Furthermore, niobium additions caused a simultaneous depression of the *liquidus* and *solidus* lines, being greater on the *solidus* than on the *liquidus* line. Another effect of niobium additions is the refinement of the as cast microstructure.

Results of magnetic measurements showed the absence of magnetism as predicted by the Schäffler diagram. Using chromium and nickel equivalents, this diagram shows that niobium additions were not sufficient to shift the steel into the ferritic field (see arrow in Fig. 18).

Elements like molybdenum, titanium and niobium are Laves phase formers, respectively Fe_2Mo, Fe_2Ti and Fe_2Nb. Silicon is known to favor also Laves phase formation [12]. In the as cast niobium containing steels, most of the niobium and silicon in the alloys are combined as Laves phase

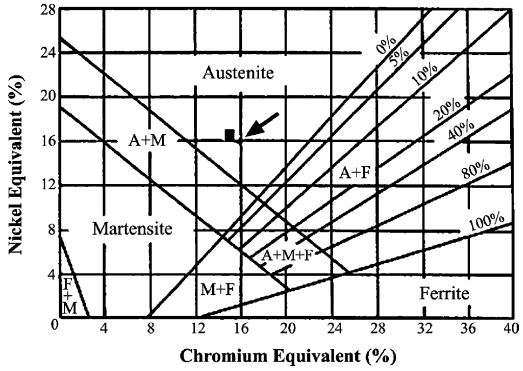

Fig. 18. Schäffler diagram [18]. The arrow indicates the region of the studied alloys Cr equiv. = %Cr + 1.4 (%Mo) + 0.5 (%Nb) + 1.5 (%Si) + 2 (%Ti) Ni equiv. = %Ni + 30 (%C) + 0.5 (%Mn) + 30 (%N).

of the type $(Fe, Ni, Cr)_2$ (Nb, Si). This formulation is reasonable since the average electron concentration of the Laves phase is 7.07, which is close to 7.0, obtained for Fe_2Nb. During solidification, the Laves phase formation consumes almost all niobium of the alloy. Laves phase formed interdendritic coarse particles, which have a low hardening effect. Furthermore, the Laves phase network causes a loss in ductility. In the as cast condition, the positive effect of niobium on hardness, yield point and strength is small as compared to its negative effect on ductility (measured through total elongation). Using the special kind of mechanical test specimen (shown in Fig. 1), it was shown that the hypothesis of nucleation and crack propagation in the Laves phases was correct.

The results of this work showed that the solid state dissolution of the Laves phase in the as cast condition is extremely difficult even at high temperatures. This can be justified by diffusion calculations. In fact, the homogenizing time (t_h) can be evaluated [19] through the following relationship

$$t_h = \frac{d^2}{D} \quad (1)$$

where t_h is the time to homogenize the ingot, d is the distance between dendrite arms (taken as 10 μm) and D is the niobium diffusion coefficient in austenite (taken as 3.25×10^{-10} cm^2/s at 1200 °C). Using this relationship, 85 h would be necessary to homogenize the ingot.

Even after mechanical processing (hot forging) and solution annealing the particles dissolution was not complete. Nevertheless the ductility of the alloys in this condition is high. Better mechanical properties of hot forged and solution annealed steels were obtained due to microstructural improvement: (i) grains were smaller than in the cast alloys; (ii) partial dissolution of Laves phase and solid solution hardening; (iii) fragmentation and rearrangement of Laves phase particles and (iv) absence of the Laves phase continuous network.

Previous research [4,12,13] has shown that Laves phase formation can occur during aging. In this work, exposure of niobium containing alloys to temperatures in the range 800–600 °C resulted in the precipitation of fine Laves phase particles, which caused significant alloy precipitation hardening. Laves phase formation in alloys containing niobium during aging heat treatments lead to an increase in hardness, mainly in aging carried out at 700 °C. At 600 °C, the increase was only observed after 100 h. In the sample aged at 800 °C an increase in hardness after the first hour could be observed. However, for aging carried out at 800 °C a decrease in hardness after about 10 h was also verified, due to coarsening (overaging) of Laves phase particles.

Within the limits of this work, rapid solidification using the melt spinning process was the only way to generate alloys free of Laves phase particles in the Fe–15% Cr–15% Ni–Nb alloys. The high hardness values of the tapes of Fe–15% Cr–15% Ni–Nb produced by melt spinning could be explained by: (i) fine grains; (ii) high vacancy supersaturation; (iii) formation of many dislocation rings; and (iv) niobium solid solution hardening. The latter hardening contribution was mainly due to the difference (over 10%) in the atomic radius.

Finally, as it has been observed in a previous work [5], niobium has a significant positive effect on the oxidation resistance of the studied alloys. Concerning the oxidation behavior of these alloys, previous work [5] has shown that niobium in solid solution reduces the oxidation rate, the scale index at high temperatures, and raises the scale breakdown temperature. The role of niobium on the oxidation of a fully austenitic stainless steels is indirect, through formation of Cr_2O_3 at the metal/metal oxide interface.

5. Conclusions

The following conclusions may be drawn from the observed data about the effects of niobium on the microstructure and mechanical properties of a fully austenitic Fe–15% Cr–15% Ni stainless steels:

1) Niobium caused depression on the *liquidus* and *solidus* temperatures, an enlargement of the solidification interval and lead to Laves phase $(Fe, Ni, Cr)_2$(Nb, Si) formation during solidification. In the as cast condition, almost all the niobium in the alloys remained concentrated in the Laves phase particles. The as cast microstructure remained almost unchanged upon solution annealing.
2) In the as cast condition, the presence of the Laves phase had a small positive effect on yield point and on tensile strength, but had a significant negative influence on the ductility of the studied steels. The Laves phase is hard and fragile and its formation between austenite dendrites causes loss of ductility.
3) Hot forging caused fragmentation, redistribution and dissolution of Laves phase particles, increasing the niobium content in the matrix, but the dissolution of Laves particles was not complete even after mechanical processing and solution annealing.

4) Only rapid solidification using the melt spinning process generated alloys free of Laves phase particles.
5) The hot forged and solution annealed alloys showed better mechanical properties than the as cast alloys.
6) Laves phase formation increased the hardness of the aged samples of niobium containing alloys. At the highest temperature (800 °C) and for longer ageing times (100 h) the hardness decreased, probably due particles coarsening.

Acknowledgments

The authors are grateful to CNPq (research fellowship no. 304611/89-1) and FAPESP (contract no. 99/10796-8) for the financial support.

References

[1] P.R. Rios, A.F. Padilha, Precipitation from Austenite Encyclopedia Materials: Science and Technology, Elsevier Science Ltd., 2001, pp. 7836–7841.
[2] A.F. Padilha, P.R. Rios, Decomposition of Austenite in Austenitic Stainless Steels (review), vol. 42, ISIJ International, Tokyo, 2002, pp. 325–337.
[3] L.G. Martinez, K. Imakuma, A.F. Padilha, Influence of niobium on stacking-fault energy of all-austenite stainless steels, Steel Res. 63 (1992) 221–223.
[4] A.F. Padilha, M. Pohl, L.V. Ramanathan, The effect of niobium addition on the microstructure of fully austenitic Fe–15% Cr–15% Ni stainless steels, Praktische Metallographie (Prac. Metallograph.) 31 (1994) 436–447.
[5] L.V. Ramanathan, M. Pohl, A.F. Padilha, The effect of niobium on the oxidation behaviour of fully austenitic Fe–15% Cr–15% Ni stainless steels, Werkstoffe und Korrosion (Mater. Corros.) 46 (1995) 71–75.
[6] A.F. Padilha, G. Schanz, K. Anderko, Ausscheidungsverhalten des titanstabilisierten austenitischen Stahls 15% Cr–15% Ni–1% Mo–Ti–B (DIN-Werkstoff-Nr. 1.4970), J. Nucl. Mater. 105 (1982) 77–92.
[7] P.V. Sivaprasad, S.L. Mannan, Y.V.R.K. Prasad, R.C. Chatuverdi, Identification of processing parameters for Fe–15 Cr–2.2 Mo-15 Ti–0.3 Ti austenitic stainless steel using processing maps, Mater Sci. Technol. 17 (2001) 545–550.
[8] W. Dienst, Hoch-Temperatur-Werkstoffe, Werkstofftechnische Verlagsgesellshaft, Karlsruhe, 1978.
[9] N. Fugita, M. Kikuchi, K. Ohmura, Expressions for Solubility Products of Fe_3Nb_3C Carbide and Fe_2Nb Laves Phase in Niobium Alloyed Ferritic Stainless Steels, vol. 43, ISIJ International, Tokyo, 2003, pp. 1999–2006.
[10] K. Yamamoto, Y. Kimura, Y. Mishima, Effect of Matrix Substructures on Precipitation of the Laves Phase in Fe–Cr–Nb–Ni System, vol. 43, ISIJ International, Tokyo, 2003, pp. 1253–1259.
[11] K. Bungart, G. Lennartz, K. Wetzlar, Einfluss des Stabilisierungsgrades auf die Ausscheidungsvorgänge niobhaltiger austenitischer Chrom-Nickel und Chrom-Nickel-Molybdän-Stähle, Archiv für das Eisenhüttenwesen 30 (1959) 429–434.
[12] A.W. Denham, J.M. Silcock, Precipitation of Fe_2Nb in a 16 wt.% Ni 16 wt.% Cr steel, and the effect of Mn and Si additions, J. Iron Steel Inst. 207 (1969) 585–592.
[13] I. Kirman, Precipitation in Fe–Ni–Cr–Nb system, J. Iron Steel Inst. 207 (1969) 1612–1618.
[14] H.-J. Kestenbach, L.O. Bueno, Effect of Fe_2Nb precipitation on the creep-properties of niobium-bearing austenitic stainless steels, Mater. Sci. Eng. 66 (1984) L19–L23.
[15] E.H. Lee, L.K. Mansur, Fe–15Ni–13Cr austenitic stainless steels for fission and fusion reactor applications II. Effects of minor elements on precipitate phase stability during thermal aging, J. Nucl. Mater 278 (2000) 11–19.
[16] G. Petzow, Metallographisches, Ätzen, Gebrüder Bornträger, Berlin, 1984.
[17] E. Schmidtmann, C. Gillessen, Einfluss unterschiedlicher Nickel- und Molybdängehalte auf die Hochtemperaturfestigkeits- und-zähigkeitseigenschaften austenitischer Chrom-Nickel-Stähle nach Abkühlung aus der Schmelze, Steel Res. 57 (1986) 69–75.
[18] A.L. Schäffler, Constitution diagrams for stainless steel weld metal, Metal Prog. 56 (1949) 680–680B.
[19] J.W. Martin, R.D. Doherty, B. Cantor, Stability of Microstructure in Metallic Systems, Cambridge University Press, Cambridge, 1997.